American Mineralogist, Volume 91, pages 413–424, 2006

Evolution of product phase assemblages during thermal decomposition of muscovite under strong disequilibrium conditions

KARINE DEVINEAU,[1,*] BERTRAND DEVOUARD,[2] FRÉDÉRIC VILLIERAS,[1] FRANÇOIS FAURE,[2] JEAN-LUC DEVIDAL,[2] AND ALAIN KOHLER[3]

[1]Laboratoire Environnement et Minéralurgie, Ecole Nationale Supérieure de Géologie, UMR INPL-CNRS 7569, 15 avenue du Charmois, BP 40, 54501 Vandoeuvre-les-Nancy cedex, France
[2]Laboratoire Magmas et Volcans, Université Blaise Pascal, UMR UBP-OPGC-CNRS 6524, 5 rue Kessler, 63038 Clermont-Ferrand cedex, France
[3]Service Commun de Microscopie Electronique à Balayage, Université Henri Poincaré, 54506 Vandoeuvre-les-Nancy, France

ABSTRACT

We investigated the thermal decomposition of muscovite in natural granite powders heated to 1175 °C for durations from 5 min to 68 h, at 1 bar, paying special attention to the early stages of decomposition. This study shows that muscovite is completely transformed after 5 min. Muscovite pseudomorphs consist of glass, mullite, and Al-rich oxides. For short durations (5 and 40 min), the Al-rich phase was identified by XRD, electron diffraction, and TEM microanalysis as γ-Al_2O_3 containing 4–8 wt% FeO (total Fe), probably a few weight percents of MgO, and possibly up to 10 wt% SiO_2. Faint superstructure spots and diffuse streaks observed in electron-diffraction patterns suggest vacancy or trace elements ordering in the γ-Al_2O_3 defect spinel structure. γ-Al_2O_3 displays an unexpected acicular morphology, elongated along three directions at 120° in the basal $(001)_{musc}$ planes and parallel to lateral faces of the former muscovite. Mullite forms rods elongated in the basal $(001)_{musc}$ planes along a direction at 90° from one set of γ-Al_2O_3 needles. The γ-Al_2O_3 structure appears to be a metastable phase that is replaced by corundum for longer durations.

Keywords: Crystal growth: mullite, Al-rich oxide, high-temperature studies, experimental petrology: granite, muscovite, electron diffraction, electron microscopy

INTRODUCTION

Weathered granites are potentially important starting products for the production of "traditional" ceramics (floor tiles, sanitaries...) because the main minerals of weathered granites, i.e., quartz, feldspars, and phyllosilicates, are indeed the main raw materials used to make these ceramics (Kingery et al. 1976). To evaluate the feasibility of using weathered granites as starting materials in the ceramic industry, we studied the mineralogical, chemical, and textural evolution of a weathered granite heat-treated at 1175 °C and room pressure (1 bar), usual conditions in ceramic works. Two main reaction mechanisms were observed: (1) partial melting and reactions involving quartz and feldspars (Devineau et al. 2005) and (2) the breakdown of muscovite. Here, we present and discuss the mineralogical breakdown of muscovite for durations of 5 min to 68 h.

Muscovite being a common accessory mineral in the ceramic products, its low-pressure and high-*T* transformations strongly influence the firing properties of ceramic products (Sundius and Byström 1953; MacKenzie et al. 1987; Barlow and Manning 1999; Cultrone et al. 2001; Rodriguez-Navarro et al. 2003). Muscovite is fully decomposed at $T \approx 980$ °C (e.g., Roy 1949), and is transformed as the *T* increases into a wide range of mineralogical assemblages including a cubic oxide phase, corundum, mullite, leucite, K-feldspars, tridymite, and glass (Roy 1949; Sundius and Byström 1953; Brindley and Maroney 1960; Eberhart 1963; MacKenzie et al. 1987; Brindley and Lemaître 1987; Barlow and Manning 1999; Cultrone et al. 2001; Rodriguez-Navarro et al. 2003). The cubic oxide phase was variously reported as "spinel," "Al-Si spinel," or γ-Al_2O_3, and its structure and chemistry have been strongly debated from many standpoints (Roy 1949; Sundius and Byström 1953; Brindley and Maroney 1960; Eberhart 1963; Brindley and Lemaître 1987). In addition to being relevant to technological applications, the mechanisms and kinetics of destabilization of muscovite are also of interest to the study of natural assemblages formed during pyrometamorphism or the ascent of xenoliths in basaltic magmas (Brearley 1986; Worden et al. 1987; Grapes 1986).

Previous works cited above usually studied the influence of *T* on muscovite decomposition. Paradoxically, only one study has been carried out, at least in part, on the kinetics of muscovite decomposition (Barlow and Manning 1999). Yet, such studies are essential to understand the disequilibrium mineralogical assemblages and to determine their transformations to reach equilibrium. In previous studies, the decomposition of muscovite has been mainly investigated by a single analytical method: powder X-ray diffraction (XRD) (Barlow and Manning 1999), petrographic microscopy (Sundius and Byström 1953), or transmission electron microscopy (Eberhart 1963; Rodriguez-Navarro et al. 2003).

The present paper proposes to complement previous works with an experimental study of product assemblages during the early stages of muscovite decomposition. The objectives were to determine the influence of short heating durations and to further

* E-mail: Karine.Devineau@ensg.inpl-nancy.fr

investigate the nature of the product phases, in particular the cubic oxide phase. The combination of different microscopies (optical, scanning, and transmission electron microscopies) has been used to observe, at various scales, the morphology of the product phases and to determine their orientation relationships within the original mica.

EXPERIMENTAL METHODS

Starting material

The starting material was a leucogranite from the Margeride pluton, French Massif Central. Leucogranites, aplites, and pegmatites occur as dikes, sills, or small stocks crosscutting the main Hercynian granite body (Pichavant and Manning 1984, see their Fig. 1). The sample chosen was collected in the Entraygues region, near the "Grangette" locality. It is a fine-grained (~0.5 mm), aplitic leucogranite, slightly weathered as indicated by its yellowish-pinkish color. The modal composition is quartz (36%), albite (21%), orthoclase (33%), and muscovite (10%). The leucogranite also contains accessory tourmaline and minor clay minerals (montmorillonite, kaolinite). Chemical analyses of the starting material are given in Devineau et al. (2005).

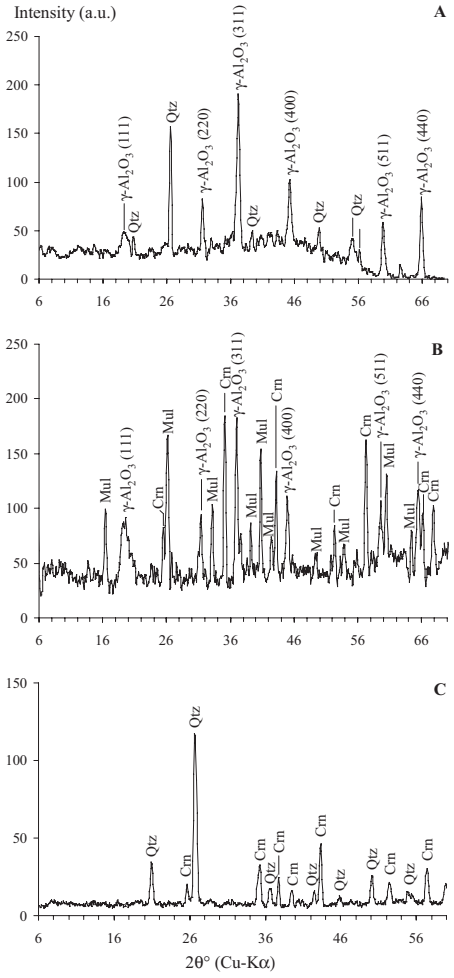

FIGURE 1. X-ray patterns digitized from films obtained by Gandolfi XRD from heated muscovite grains extracted by microdrilling from samples heated for (**a**) 40 min and (**b** and **c**) 24 h. Minor mullite reflections were also observed on the Gandolfi film from sample in **c**, but are not visible on the digitized spectrum. Mul = mullite, Crn = corundum, and Qtz = quartz.

Experimental procedure

The Grangette leucogranite was powdered to grain sizes ranging from <3 to ~200 μm, with 50% of particles being <30 μm. The wet powder was cold pressed into a cylindrical shape (length = 24 mm, diameter = 23 mm). Cylinders were placed directly in a muffle furnace (Veckstar) previously equilibrated at the desired *T*. Six heat-treatment experiments were carried out at 1175 °C in air (P = 1 bar), for run durations of 5, 10, and 40 min and 3, 24, and 68 h. The *T* of the furnace was checked continuously with a $Pt/Pt_{10}Rh$ thermocouple, with an accuracy of ±5 °C. At the end of the experiments, samples were removed from the furnace and quenched in air. The initial high porosity of samples (≈40%) and the consistency of the results allowed us to be confident that the experimental *T* had been reached throughout the whole sample even for the shorter run durations.

Analytical methods

XRD patterns were obtained from powders of starting material and heat-treated samples using a D8 Bruker diffractometer with Co$K\alpha_1$ radiation. In addition, XRD was performed with a Gandolfi chamber (Cu$K\alpha_1$ radiation) on single crystals of muscovite (~100 μm) extracted from thick (200 μm) sections of the heated samples using a Medenbach microdrill mounted on a conventional optical microscope (e.g., see Paquette et al. 2004 for illustrations of the procedure). The films obtained from Gandolfi diffraction were digitized, and intensity profiles were extracted using the NIH Image software.

Petrographic thin sections (30 μm thick), prepared from both untreated and heat-treated samples, were examined by transmitted- and reflected-light microscopy and by scanning electron microscopy (SEM) using backscattered electron (BSE) imaging on a Hitachi 2500 microscope (Université Henri Poincaré, Nancy, France) operated at 20 kV accelerating voltage. Microanalyses were acquired on the SEM with a ThermoNORAN Vantage energy dispersive X-ray spectrometer (EDS) equipped with a polymer window.

For transmission electron microscope (TEM) work, dismountable thin sections were prepared using CrystalBond thermal resin. Heated muscovite grains were selected after careful observation by petrographic microscopy and Cu single-hole TEM grids were glued on the areas of interest. Samples were then separated from the quartz-feldspar matrix with a scalpel under a binocular microscope, and finally unglued from the glass slide and cleaned with acetone. TEM samples were thinned to electron transparency using a Gatan dimpler and ion-beam milling (Gatan PIPS). Samples were C-coated to prevent charging. Observation was made with a JEOL 2000fx TEM (CRMCN facility, Marseille, France) operated at 200 kV and microanalyses were acquired with a Si(Li) detector fitted with a UTW and a TRACOR Northern 5500 EDS system. Spatial resolution for the EDS/TEM microanalysis was ~10 nm.

Major-element analyses of minerals and glasses were obtained using a Cameca SX100 electron microprobe (Université Blaise Pascal, Clermont-Ferrand, France). Operating conditions were 15 kV accelerating voltage, 5 nA beam current, and 10 s counting times on peak. Standards used were natural albite, orthoclase, olivine, wollastonite, synthetic Fe_2O_3, Al_2O_3, and $MnTiO_3$. PhiRhoZ correction procedures were applied. A focused beam (spot size 1 μm) was used for the starting material. For heat-treated samples, the analyses were performed with a defocused beam (5 μm) to minimize the migration of alkalis.

RESULTS

XRD patterns

The main result obtained by powder XRD is the disappearance of the peaks from muscovite after 5 min of heating. Feldspars disappear completely between 40 min and 3 h (Devineau et al. 2005), then only diffraction peaks from quartz are observed.

Gandolfi diffractions of heated muscovite grains (Fig. 1) show the following results. For run durations of 5 min, no peaks from muscovite or from product phases were observed. Only peaks from quartz were detected, corresponding to impurities around the extracted muscovite. Faint reflections that could possibly be attributed to feldspars were observed, and these probably are impurities from the starting granite. After 40 min (Fig. 1a), peaks appear that can be indexed as a spinel structure. As mentioned in the introduction, the nature of this cubic phase has been much debated. Taking into account the other observations reported

below, we index these reflections as γ-Al_2O_3 (see discussion). After 24 h, two heated muscovite grains yielded somewhat different results (Figs. 1b and 1c): in Figure 1b, mullite + corundum (=α-Al_2O_3) + γ-Al_2O_3 were observed simultaneously, whereas in Figure 1c, corundum is by far the most abundant phase. From the Gandolfi patterns, 111 reflections from γ-Al_2O_3 invariably appear broadened, but other reflections are reasonably sharp.

Petrographic microscopy

The initial muscovite shows the characteristic optical properties of white micas. The content of Fe in the starting muscovite (>2 wt% total Fe oxide), however, causes light-yellow to green colorations and pleochroism in lateral sections.

For all run durations at 1175 °C, the lath-like shape of the original mica is preserved but optical properties vary. In plane-polarized light, heated muscovite remains pleochroic and becomes slightly yellow to light-brown colored for 5 and 40 min (Fig. 2a), then light to dark gray for 24 h (Fig. 2b). Numerous micrometer-sized, needle-shaped crystals are observed parallel to the direction of former cleavages of muscovite from 40 min, as the heated muscovite changes from transparent to translucent. Under crossed polars, the birefringence of the heated muscovite appears to be lower (yellow tints for 5 and 40 min, brown with pinkish hues for 24 h) but the extinction remains parallel. Sundius and Byström (1953) were the first authors to observe similar changes in heated muscovite, which they defined as muscovite "pseudomorphs." Our muscovite pseudomorphs also display the "cellular structure" as defined by Tite and Maniatis (1975) due to the presence of bubbles (Fig. 2). This texture also has been reported in the recent studies of Cultrone et al. (2001) and Rodriguez-Navarro et al. (2003). The formation of bubbles in muscovite pseudomorphs is discussed in Devineau (2002).

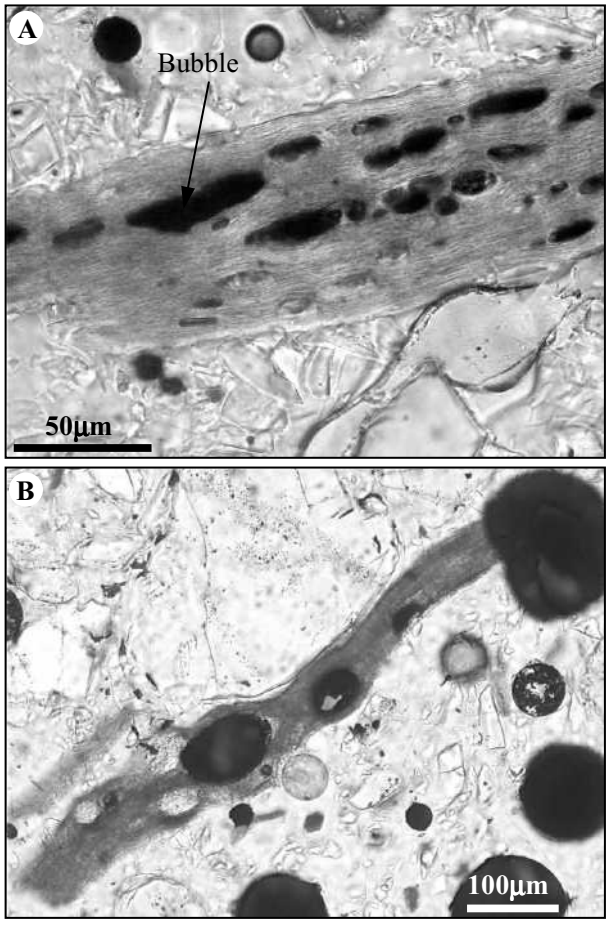

FIGURE 2. Optical micrographs (plane-polarized light) of muscovite heated for (**a**) 40 min and (**b**) 24 h.

Scanning electron microscopy

BSE images of heated muscovite grains (Figs. 3, 4, and 5) display product phases for all run durations. Even at the SEM scale, no relics of the original muscovite can be recognized within the pseudomorphs. The contrast between the product phases and the matrix indicates that the crystals consist of chemical elements with higher mean atomic number than the matrix. The size of the crystals is difficult to determine with the SEM because they are fine-grained and overlap each other. Moreover, lengths are only apparent as they depend on the orientation of the crystals relative to the sample surface. Therefore, the sizes given below are only estimates and do not represent a mean value or the size of the biggest observed crystal. After 24 and 68 h, the matrix clearly appears as a homogeneous melt in the lateral sections and presents zones large enough to attempt microprobe analyses. The EDS analyses carried out on product minerals suggest that they are Al-Si oxides; however, because their width is always ≤1 µm, analyses are systematically contaminated by the melt.

Observations in lateral sections

In lateral sections of heated muscovite grains (Fig. 3), most product phases appear to be needle shaped and parallel to the former cleavages of muscovite, except in the vicinity of bubbles where they deviate. After 5 (Fig. 3a) and 10 min, needles (≤100 nm thickness) are numerous and not quite individualized at the SEM scale. After 40 min (Fig. 3b), the needles become large enough (0.2 × 5 µm) to be observed properly at the SEM scale. Most crystals (labeled as A) are parallel to the former cleavages but a few needles (labeled as B) display a different orientation, roughly at 120°. Those B needles appear shorter (0.2 × 1.8 µm) than A needles, possibly because they are not parallel to the surface of the section. After 3 h (Fig. 3c), the muscovite pseudomorphs consist of (1) well individualized A needles (0.3 × 7 µm) and a few B needles (0.3 × 2.75 µm); and (2) cloudy zones (Fig. 4a) formed by fine needles with similar orientation to A and B needles and few blocky-looking crystals (0.45 × 0.45 µm). After 24 h, the sizes of all phases increase: 1 × 12 µm for A needles, 0.8 × 6 µm for B needles (Fig. 3d), and 0.6 × 1 µm for the blocky-looking, sometimes hollow minerals within the cloudy zones (Fig. 4b). For this run duration, the larger needles tend to be surrounded by glass devoid of smaller needles (cloudy zones) (Fig. 4c). After 68 h, the cloudy zones seem to have disappeared and only large A needles (0.5 × 11 µm) and a few B needles (0.4 × 4 µm) are observed within the glass (Fig. 3e). Rare larger crystals (e.g., arrowed in Fig. 4d) can be assigned to the phase previously referred to as "blocky crystals."

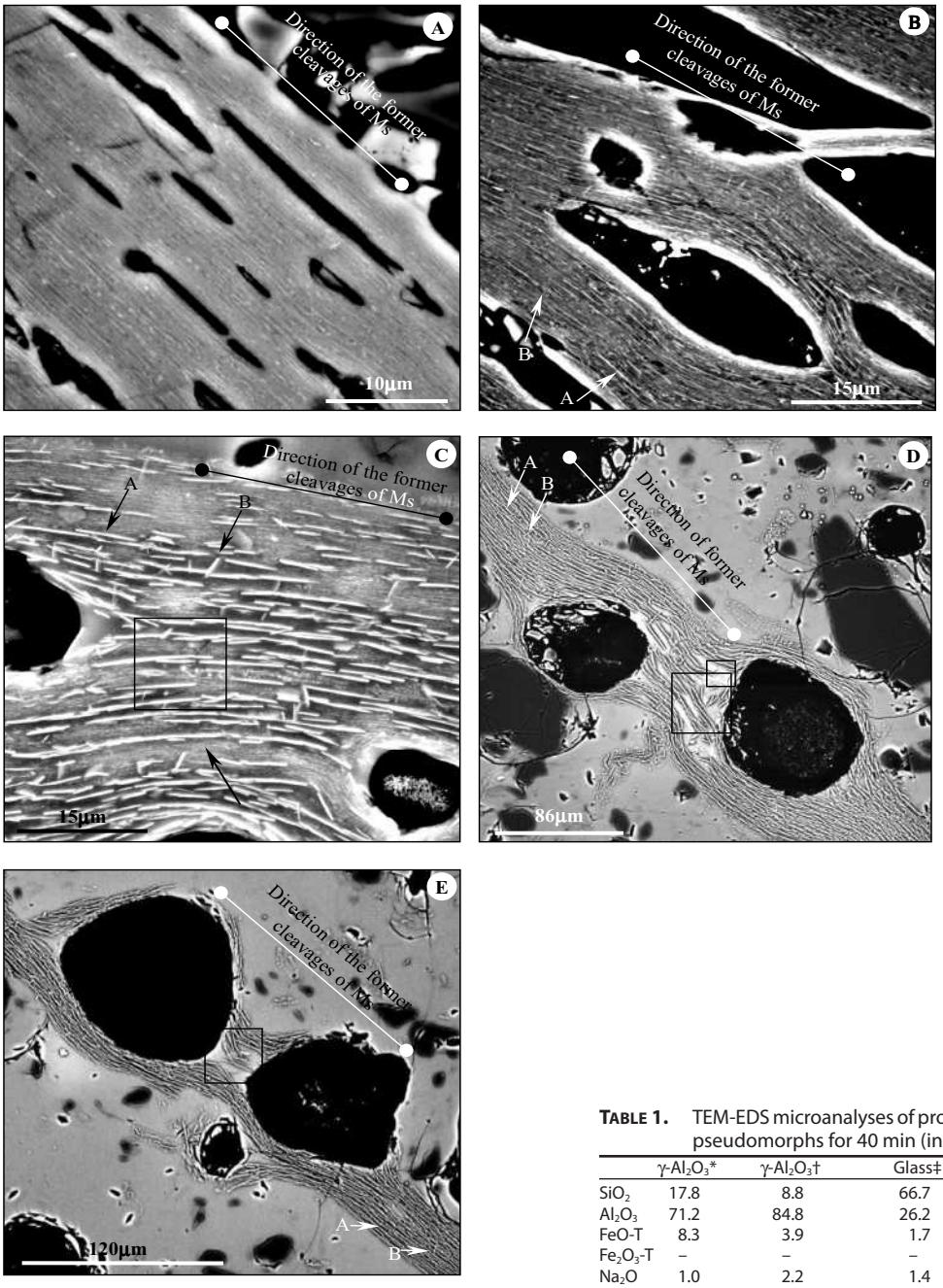

FIGURE 3. BSE-SEM images showing lateral sections of muscovite heated for (**a**) 5 min, (**b**) 40 min, (**c**) 3 h, (**d**) 24 h, and (**e**) 68 h. Muscovite (Ms) is replaced completely by glass and micrometer-sized product phases, mainly needles parallel to the direction of the former muscovite cleavages (labeled A) and sometimes, oriented at roughly 120° relative to the direction defined by the A needles (labeled B). The size of the needles increases with the run duration. Bubbles inside the muscovite pseudomorphs (dark areas on all images) deviate the needles in their vicinity.

Observations in basal sections

In basal sections (Fig. 5), product phases are difficult to observe with the SEM for 5, 10, and 40 min experiments, and no preferential orientation can be ascertained for these durations. The needles become larger and better individualized as the run duration increases. After 68 h, the basal sections of the muscovite pseudomorphs (Fig. 5a) clearly consist of numerous needles (0.7 × 14 µm) oriented at 120° along three directions parallel to the faces of the former muscovite crystal (Fig. 5b). A few larger, rod-shaped crystals (2 × 23 µm) can be observed with a direction of elongation at 90° from one of three directions defined by the needles (Fig. 5b).

TABLE 1. TEM-EDS microanalyses of product phases from muscovite pseudomorphs for 40 min (in oxide wt%)

	γ-Al_2O_3*	γ-Al_2O_3†	Glass‡	Mullite*	Mullite†
SiO_2	17.8	8.8	66.7	26.2	26.6
Al_2O_3	71.2	84.8	26.2	67.5	67.4
FeO-T	8.3	3.9	1.7	–	–
Fe_2O_3-T	–	–	–	3.2	3.4
Na_2O	1.0	2.2	1.4	2.2	2.2
K_2O	1.0	0.1	3.2	0.7	0.1
CaO	0.7	0.1	0.8	0.3	0.3
Total	100	100	100	100	100
	Formulae based on 32 O atoms			Formulae based on 13 O atoms	
Si	3.3	1.6		1.9	1.9
Al	15.7	18.4		5.8	5.8
Fe	1.3	0.6		0.2	0.2
Na	0.4	0.8		0.3	0.3
K	0.2	0.0		0.1	0.0
Ca	0.1	0.0		0.0	0.0
Sum	21	21.4		8.3	8.2

* Analysis of one particle.
† Average of two to four analyses carried out on the same particle.
‡ Average of three analyses. For mullite, the Fe content is reported as F_2O_3, since it is the likely oxidation state of Fe incorporated in this structure.

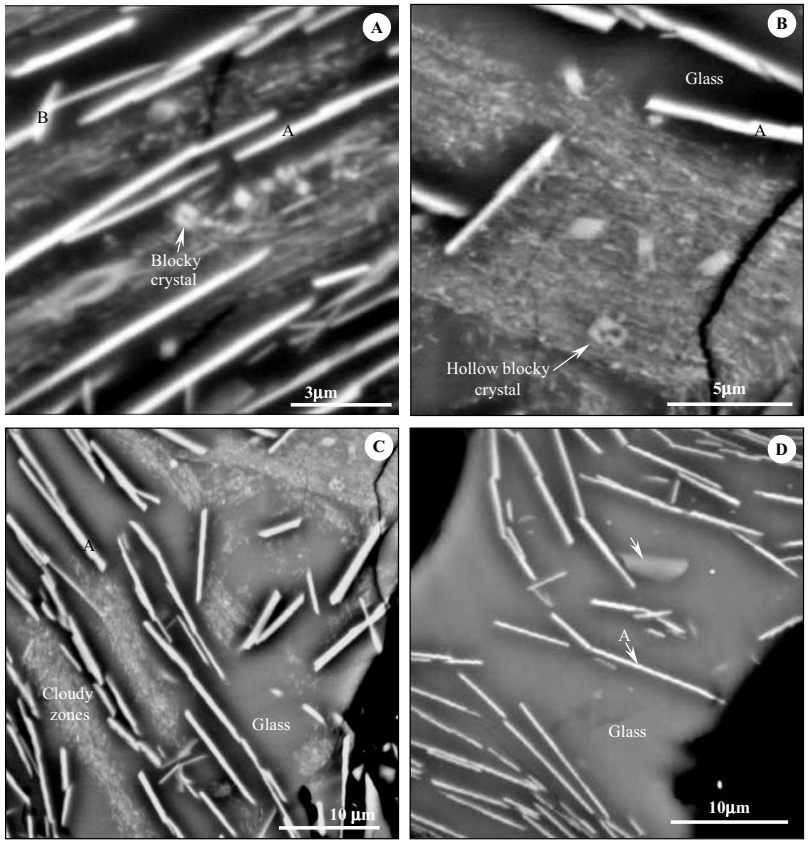

FIGURE 4. BSE-SEM enlargements of the areas marked in Figure 3. (**a**) After 3 h, enlarged from Figure 3c, small cloudy zones appear between the large needles and they consist of fine needles not quite individualized with the same orientation of large needles and few small blocky-looking, commonly hollow, crystals. (**b** and **c**) After 24 h, enlarged from Figure 3d, part of the matrix clearly appears for the first time as a homogeneous melt. Cloudy zones consisting of fine needles remain, but tend to disappear in the vicinity of the larger needles. (**d**) After 68 h, enlarged from Figure 3e, the cloudy zones are no longer observed and the muscovite pseudomorph consists only of large needles within a glass. The larger crystal (arrowed) could be the same species that was described as "blocky" in **a** and **b**.

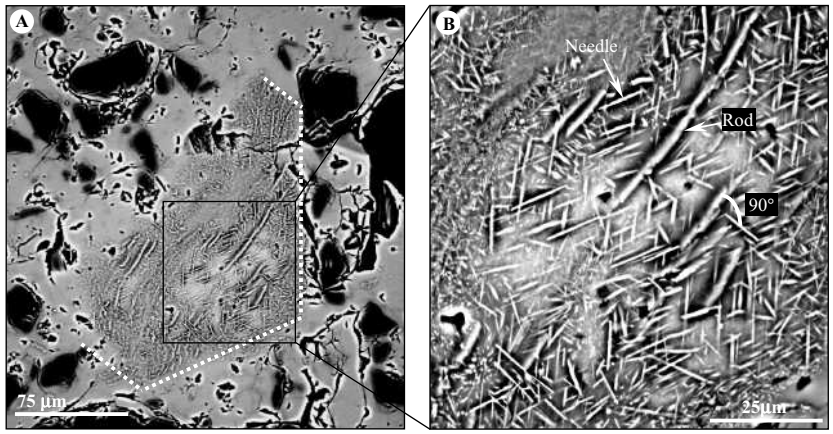

FIGURE 5. BSE-SEM image of a basal section of muscovite heated for 68 h. (**a**) Lower magnification, showing part of the former muscovite lateral faces (outlined by a dotted line). (**b**) Enlargement of the area framed in **a**, showing that the numerous needles are oriented at 120° along directions parallel to the lateral faces of the former muscovite crystal. Few larger, rod-shaped crystals are elongated at 90° from one of three directions defined by the needles.

Transmission electron microscopy

Conventional TEM images, selected area electron diffraction (SAED) patterns, and EDS microanalyses were recorded from lateral sections of heated muscovite at 5 and 40 min. TEM shows that the former muscovite is transformed completely to melt, numerous acicular crystals, and a few blocky minerals (Fig. 6). SAED patterns of the needles can be indexed as a spinel structure, which we ascribe to γ-Al_2O_3 (see discussion). EDS analyses (Table 1) indicate an Al or Al-Si oxide. Due to the small width of these crystals (~10 nm), most analyses are probably contaminated by the surrounding melt. However, analyses from the larger crystals (up to 50 nm in the 40 min sample) display minor-element contents different from the adjacent melt, suggesting that these analyses are not contaminated very much. These analyses indicate maximum SiO_2 contents of 8–17 wt% in γ-Al_2O_3, and significant enrichment in FeO (4–8 wt%) compared to the melt (Table 1). Most γ-Al_2O_3 needles are parallel and only a few needles are arranged to roughly 120° relative to these principal directions (Figs. 6a, 6b, and 6c), similarly to what was observed by SEM for longer durations. All the needles display the same diffraction contrast, and SAED indicate that the crystals share a similar crystallographic orientation. When needles are oriented perpendicularly to the beam (Fig. 6c), the SAED patterns correspond to a $[\bar{1}12]$ zone axis and indicate that the needle-shaped

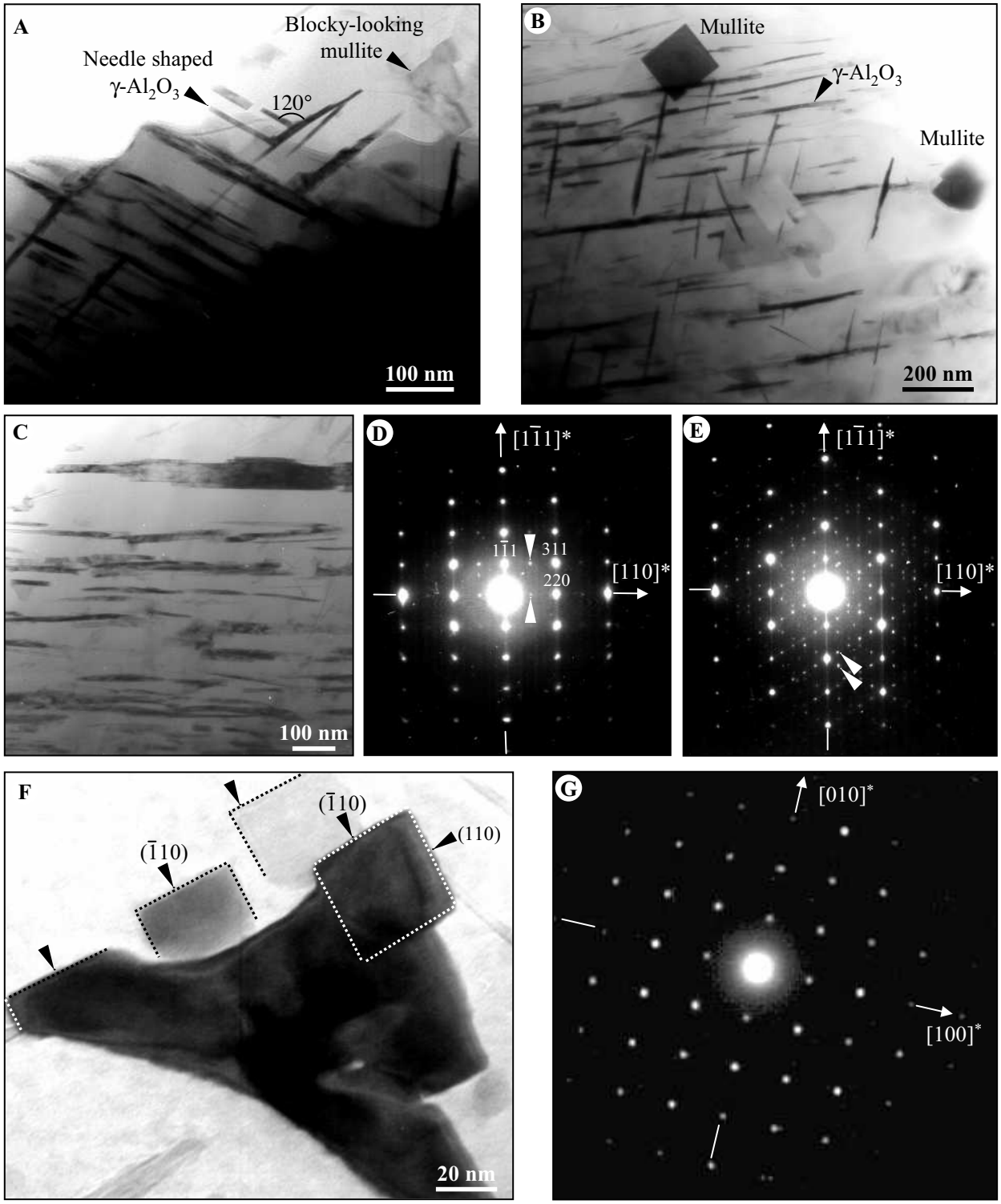

FIGURE 6. Conventional TEM images showing reaction products in muscovite heated for 5 and 40 min at 1175 °C. (**a** and **b**) Bright-field images showing needle-shaped crystals identified as γ-Al_2O_3 and blocky-looking mullite, for 5 min and 40 min, respectively. (**c**, **d,** and **e**) Bright-field image and SAED patterns of needle-shaped crystals (5 min). The SAED patterns are indexed as γ-Al_2O_3, but also show faint superstructure spots (arrowed) and diffuse streaks along the [1$\bar{1}$1] direction. (**f** and **g**) Bright-field image and SAED pattern of a mullite section with a skeletal shape made of squarish crystallites.

crystals are elongated along a [110] direction (Fig. 6d). The broadening of 111 reflections observed from Gandolfi XRD is consistent with the fact that half the {111} faces would be in a zone axis around the direction of elongation, i.e., correspond to the smallest dimension of the needles. In addition to the reflections expected from the γ-Al_2O_3 spinel structure, faint reflections defining superstructures (arrowed in Figs. 6d and 6e) and streaks along [1$\bar{1}$1] were occasionally observed in some crystals.

SAED patterns from the "blocky" minerals (Fig. 6f) correspond to mullite (Fig. 6g). EDS analyses (Table 1) indicate a restricted range of chemical composition consistent with mullite containing ~3 wt% Fe_2O_3. The analyses are consistent with stoichiometric mullite (as opposed to peraluminous mullites, Cameron 1977). The Fe contents are similar to those reported in the literature (Rodriguez-Navarro et al. 2003; Brearley and Rubie 1990; Rubie and Brearley 1987; Worden et al. 1987; Brearley 1986; Grapes 1986), which usually range from 1 to 5 wt% Fe_2O_3. Mullite sections oriented along the [001] zone axis are limited by {110} and {$\bar{1}$10} faces, which is the common morphology for this mineral (e.g., Deer et al. 1982). However, the aspect of mullite sections in this orientation differs for 5 and 40 min. After 5 min (Fig. 6f), mullite sections display a dendritic shape that consist of square crystallites ~30 nm. All crystallites share a common crystallographic orientation, as indicated by SAED. After 40 min, mullite sections (~100 nm) have a more definite {110} + {$\bar{1}$10} morphology (Fig. 6b), with rare subgrain boundaries.

Table 2. Electron-microprobe analyses (oxide wt%) of starting muscovite and muscovite pseudomorphs in the heat-treated samples

	Before heating*	5 mn†	10 mn†	40 mn†	3 h‡	24 h‡	68 h‡
SiO_2	45.65	48.40	48.55	48.06	50.54	54.96	64.08
Al_2O_3	34.32	35.85	36.70	36.12	34.82	31.94	21.25
Na_2O	0.58	2.63	3.86	4.38	4.18	4.19	4.75
K_2O	10.50	8.61	6.86	5.94	5.61	5.35	6.34
CaO	0.01	0.04	0.08	0.21	0.51	0.61	0.99
FeO-T	2.35	2.37	2.48	2.58	2.26	1.76	1.39
TiO_2	0.50	0.49	0.36	0.54	0.55	n.d.	n.d.
MgO	1.02	0.96	0.87	1.09	0.95	0.74	0.60
MnO	0.09	0.09	0.10	0.11	0.14	0.00	0.04
Total	95.02	99.44	99.88	99.03	99.56	99.55	99.44
			Formulae based on 22 O atoms				
Si	6.14	6.18	6.14	6.12	6.36	6.83	7.94
Al	5.43	5.38	5.46	5.41	5.15	4.67	3.10
Na	0.15	0.65	0.94	1.08	1.02	1.01	1.14
K	1.80	1.40	1.11	0.97	0.90	0.85	1.00
Ca	0.00	0.01	0.01	0.03	0.07	0.08	0.13
Fe	0.26	0.25	0.26	0.27	0.24	0.18	0.14
Ti	0.05	0.05	0.03	0.05	0.05	n.d.	n.d.
Mg	0.21	0.18	0.16	0.21	0.18	0.14	0.11
Mn	0.01	0.01	0.01	0.01	0.01	0.00	0.00
Sum	14.05	14.11	14.13	14.15	13.98	13.76	13.58

* Average of seven analyses.
† Average of 8 to 16 bulk compositions (crystalline phases and glass) of muscovite pseudomorphs.
‡ Selected analyses with highest SiO_2 content, considered to be best representative of glass compositions.

Electron microprobe

Table 2 lists electron microprobe analyses carried out on lateral sections of starting muscovite and muscovite pseudomorphs. For the short heat treatments (5, 10, and 40 min), average analyses correspond to the bulk compositions of muscovite pseudomorphs (crystals and glass) because these different phases were too small to be analyzed separately. In contrast, analyses from the longer heat treatments (3, 24, and 68 h) favor the measurement of chemical compositions of the glass, but cannot be considered devoid of contamination by product phases, due to the restricted areas of melt (typically <5 μm across even at 68 h). Thus, for these long heat treatments, the analysis with the highest SiO_2 content, considered to be the best representative of glass composition, has been selected for Table 2. All analyses are plotted on SiO_2-Al_2O_3-K_2O diagrams (Fig. 7).

For the shorter heat treatments, bulk compositions of muscovite pseudomorphs show a progressive decrease in K_2O (from 11 to 6 wt%) and increase in Na_2O (from 0.6 to 4.5 wt%) relative to the starting muscovite (Table 2). On the other hand, the SiO_2, Al_2O_3, and other minor elements (CaO, FeO, TiO_2, MgO, and MnO) contents do not vary noticeably with the heat treatment. Analyses of the starting muscovite and muscovite pseudomorphs are well grouped, indicating rather homogeneous compositions (Fig. 7b). For the longer heat treatments (Fig. 7c), analyses are scattered between a composition close the bulk at 40 min and a glass composition enriched in SiO_2, up to 65 wt% for the highest values at 68 h (Table 2). This trend is certainly due to contamination, representing a mixing between the composition of the glass and the bulk composition (including product phases). For comparison, TEM analyses of glass at 40 min yielded SiO_2 contents ~65%. This finding is consistent with the extreme compositions measured by microprobe at 68 h, which are considered to be the best representatives of melt compositions. This result suggest that the melt composition may be about constant from 40 min to 68 h. Figure 8 shows the evolution of FeO and MgO contents vs. SiO_2. The more SiO_2-enriched analyses, which are more representative of the glass and best measured for the longer durations, are noticeably depleted in Fe and Mg, thus confirming the observation by analytical TEM that these elements are preferably incorporated in the product phases. The BSE contrast of the γ-Al_2O_3 needles also suggest an enrichment in Fe: as the backscattering coefficients of SiO_2 and Al_2O_3 are not very different, the observed contrasts probably reflect the FeO concentrations of the different phases.

Discussion

High-*T* decomposition products of muscovite

Combining the results of XRD and TEM, thermal destabilization of muscovite results an Al-rich phase with a spinel structure, mullite, corundum, and melt. The assemblage Al-rich "spinel" phase + mullite + melt is observed for durations as short as 5 min. Barlow and Manning (1999) reported complete transformation of muscovite for 10 min, but no shorter experiments had been reported so far. At 5 min, product phases were not evidenced by Gandolfi XRD but they are unambiguously observed by SEM and TEM. From Gandolfi XRD, the "spinel" phase appears to be dominant up to 40 min, then the proportion of mullite increases between 40 min and 24 h. Corundum appears at 24 h, apparently at the expense of the Al-rich "spinel" phase and possibly mullite.

On the basis of the K_2O-Al_2O_3-SiO_2 equilibrium phase

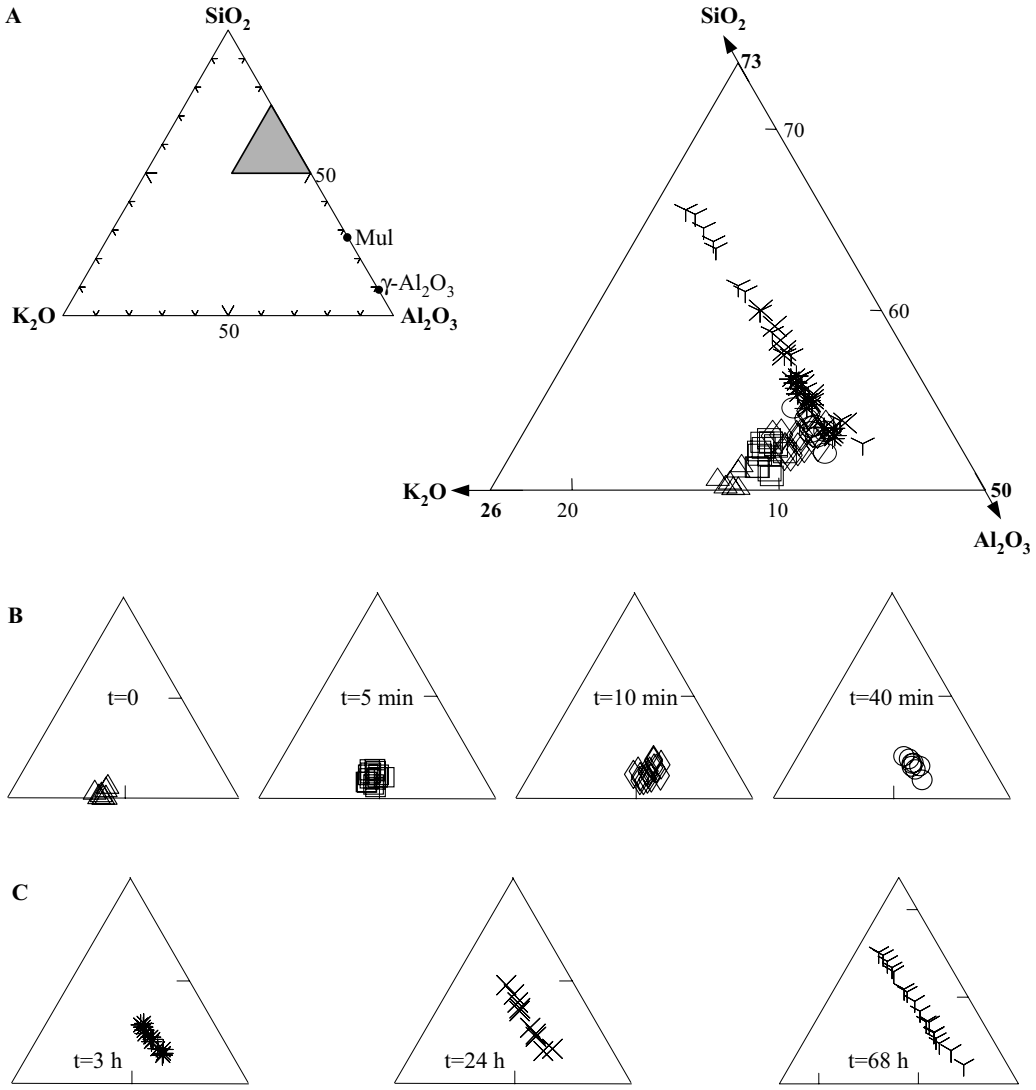

FIGURE 7. Electron microprobe analyses of the starting muscovite and muscovite pseudomorphs, projected in the SiO_2-Al_2O_3-K_2O system. (**a**) Left: Shaded area defining the small portion of the triangle that is used in the rest of the Figure, and compositions of mullite and γ-Al_2O_3 product phases from TEM-EDS analyses in Table 1. Right: All microprobe analyses for the various durations. (**b**) Microprobe analyses plotted separately for starting muscovite and increasing durations from 5 to 40 min. These analyses represent bulk compositions from the muscovite pseudomorphs, due to the sub-micrometer size of the product phases. (**c**) Microprobe analyses plotted separately for durations from 3 to 68 h. These analyses favor the composition of the glass, but are nevertheless contaminated by product phases (see text).

diagram (Yoder and Eugster 1955), the anhydrous muscovite composition should give leucite + K-feldspar + mullite below 1140 °C, leucite + mullite + melt from 1140 to 1315 °C, and leucite + corundum + melt above 1315 °C. However, a large range of assemblages has been described by various authors (Roy 1949; Sundius and Byström 1953; Brindley and Maroney 1960; Eberhart 1963; MacKenzie et al. 1987; Barlow and Manning 1999; Cultrone et al. 2001; Rodriguez-Navarro et al. 2003). Commenting on this fact, Brindley and Lemaître (1987) wrote in their review that the product phases are mainly those to be expected from the equilibrium diagrams, but the association and the proportion of phases vary with the precise chemical compositions of the micas and the heat treatments employed. In our experiments, neither leucite nor K-feldspar were observed. In practice, leucite is seldom recorded as a decomposition product (Brindley and Maroney 1960). It has nevertheless been observed in some recent experiments (e.g., Barlow and Manning 1999). The loss of K_2O that we observed may be a reason for the absence of K-rich phases. This decrease in K_2O has been observed by many authors (Eberhart 1963; Grapes 1986; Sanchez-Navas

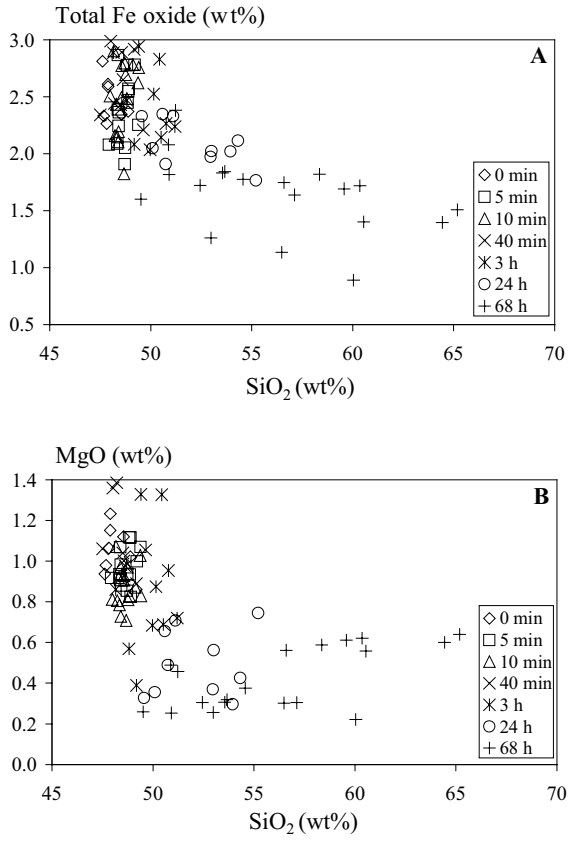

FIGURE 8. Evolution of the (**a**) total Fe oxide and (**b**) MgO contents as a function of SiO_2 in the starting muscovite and the muscovite pseudomorphs for different run durations.

1999; Cultrone et al. 2001; Rodriguez-Navarro et al. 2003) and is attributed to the departure of K^+ with water along the cleavages planes of the muscovite during the dehydroxylation stage. We also noted an increase in the amount of Na_2O. Those transfers of elements should take place between the reacting phyllosilicates and the surrounding feldspars, partially molten during the short heat treatments in our experiments (Devineau et al. 2005), as suggested by Worden et al. (1987).

A spinel-structure phase has been early described by various authors as a product of the thermal decomposition of phyllosilicates, mainly muscovite (Roy 1949; Sundius and Byström 1953; Brindley and Maroney 1960; Eberhart 1963; MacKenzie et al. 1987; Brindley and Lemaitre 1987; Barlow and Manning 1999) and kaolinite (e.g., Brindley and Nakahira 1959; Leonard 1977; Brindley and Lemaître 1987; Low and McPherson 1988; Srikrishna et al. 1990; Lee et al. 1999; Lee et al. 2001). It is described by Brindley and Lemaître (1987) as being among the first products formed during the thermal decomposition of muscovite. This phase is not expected from the equilibrium phase diagram, and it is considered to be metastable and transitional. In our samples, it disappears, at least in some crystals, for 24 h, as in the experiments of Barlow and Manning (1999). The nature of this spinel-type phase has been largely debated in the literature (Sundius and Byström 1953; Brindley and Maroney 1960; Eberhart 1963; Nicol 1964; MacKenzie et al. 1987). It is often identified to γ-Al_2O_3 (which has a defective spinel structure), but its precise composition is still unclear since it is very difficult to distinguish between $MgAl_2O_4$ (spinel *s.s.*) and γ-Al_2O_3 on the basis of XRD or SAED (Eberhart 1963), and crystals are usually too small for microanalysis. There is suspicion that it may contain significant Si: Brindley and Nakahira (1959) proposed the structural formula Si_8 $[Al_{32/3}\square_{16/3}]$ O_{32} ($\square$ = vacancy) for spinel phases from heated kaolinites, and Eberhart (1963) suggested Si_8 $[Al_8\square_8]$ $[O_{28}\square_4]$ for spinel phases from decomposed end-member muscovite. Most other authors simply refer to γ-Al_2O_3, from diffraction data, without addressing the question of its composition. Mackenzie et al. (1987), from a combined XRD-NMR study of heated muscovite, conclude that the spinel phase contains considerably less Si that suggested by Eberhart, if any at all. Our study suggests that the γ-Al_2O_3 phase does contain some SiO_2 and also incorporates some Fe (up to 8 wt% FeO) and Mg, but that the maximum Si content is probably around 10 wt% SiO_2, much lower than proposed by Eberhart. McHale et al. (1997) experimentally demonstrated the existence of an Al_2O_3-SiO_2 solid solution with the γ-Al_2O_3 structure, up to at least 10 wt% SiO_2. They also showed from calorimetry measurements that γ-Al_2O_3 is metastable, relative to corundum + quartz, over this compositional range. The γ-Al_2O_3 spinel phase occurring in heated muscovite might thus be enriched in SiO_2, but is not a definite compound, and appears to be a transitional phase that transforms to corundum. Sundius and Byström (1953) and Grapes (1986) discussed the influence of oxide impurities on the formation of product phases and suggested that Fe impurities in muscovite promote the formation of Al-rich phases (γ-Al_2O_3 then corundum). This may explain why γ-Al_2O_3 is systematically present in our samples (>2 wt% total Fe oxide in the starting muscovite) for short heating durations, and why corundum seems to be a stable product despite the fact it is not expected at this temperature from the K_2O-Al_2O_3-SiO_2 phase diagram. Moreover, in our experiments, the samples were submitted to severe conditions of disequilibrium. It is known that under such conditions, the thermodynamically stable paragenesis is generally not observed. Instead, the crystallization of the stable assemblage proceeds via precursor phases (Ostwald step rule; Putnis and McConnell 1980). The formation of an oxide phase rather that the expected mullite is consistent with this behavior, because it probably is easier, energetically speaking, to form a binary oxide rather than a complex Al-silicate phase.

γ-Al_2O_3 has a defect spinel structure because part of the tetrahedral or octahedral sites, which are usually occupied in the structure of the spinel, *s.s.* are vacant [suggested stoichiometry of $(Al_{64/3}\square_{8/3})$ O_{32}]. γ-Al_2O_3 is part of a family of so-called "transition aluminas" (δ-, χ-, κ-, η-, θ-, and γ-Al_2O_3) that have been studied extensively because they are important materials used in composites materials and as catalysts or catalyst supports (e.g., Zhou and Snyder 1991; Souza-Santos et al. 2000). The transition aluminas are metastable phases that tend to transform into the stable α-Al_2O_3 (= corundum) structure. All transition alumina structures differ by the arrangement of the Al atoms in the interstitial sites of a close-packed O sublattice (Levin and Brandon 1998). Despite extensive studies of the γ-Al_2O_3 structure, the exact symmetry and location of the vacancies in its spinel-type structure are still disputed (e.g., Gutierrez et al.

2001, and references therein; Gan and O'Connor 1996). To account for the fact that no superstructure is observed by XRD, it is usually assumed that vacancies are distributed randomly. Alternatively, other authors (e.g., Han et al. 1995; Kryukova et al. 2000) have argued that the vacancies are segregated in stacking faults. To the best of our knowledge, only Eberhart (1963) reported a possible superstructure reflection in γ-Al_2O_3 (which he attributed to the ordering of Si in the structure). In the present study we observed diffuse streaks along the $[1\bar{1}1]$ direction and faint superstructure spots in some SAED patterns from γ-Al_2O_3 (Fig. 6). The diffuse streaks may originate from stacking faults or from incomplete ordering. We could not attribute the superstructure spots observed in some crystals (Figs. 6d and 6e) to another transition alumina structure, and we propose that they may originate from the ordering of vacancies, or possible Si, in the γ-Al_2O_3 structure. This suggests that ordering may be possible for this phase, but it is to be noted that it is far from being systematic, and that these superstructures were found to be variable within the same needle.

Mutual orientation of product phases

The shape and organization of the product phases within the pseudomorphs of heated muscovite are similar at the micro- (SEM) and nano- (TEM) scales. The TEM work has allowed us to identify the crystalline phases and characterize their morphology, but no additional phase or reaction textures have been observed. Comparing SEM with TEM results, we conclude that the needles observed by SEM are γ-Al_2O_3, whereas the larger rods with rectangular or skeletal sections are mullite.

In previous studies, the orientation relationships between the original muscovite and the product phases such as mullite (Eberhart 1963; Worden et al. 1987; Brearley and Rubie 1990; Rodriguez-Navarro et al. 2003) or spinel-type phases (Eberhart 1963; Worden et al. 1987) were determined from XRD and TEM work. These determinations were possible because relics of unreacted muscovite and product phases co-existed inside the muscovite pseudomorphs. All authors noticed strong topotactic orientations of mullite and spinel phase with muscovite, with $[001]_{mul}$ // $[010]_{musc}$, $(111)_{spinel}$ // $(001)_{mica}$, and $[110]_{spinel}$ // $[010]_{musc}$. In addition, Rodriguez-Navarro et al. (2003) reported that $(120)_{mul}$ or $(210)_{mul}$ are subparallel to $(001)_{musc}$, in accordance with Eberhart (1963). We noticed in our study that, despite the fact that the muscovite is completely decomposed in 5 min, product phases retain crystallographic orientations for up to 68 h that can only be inherited from the precursor muscovite. This confers optical properties to the muscovite pseudomorphs that derive from those of the product assemblages. As interpreted by previous authors, these orientation relationships can be explained by the topotactic nucleation of the reaction products within the dehydroxylated muscovite lattice. Eberhart observed that the spinel phase formed at 800 °C, far below the melting temperature. Rodriguez-Navarro et al. (2003) suggested that the growth of mullite was promoted by the development of supersaturated melt pockets oriented parallel to the basal planes of muscovite. In our study, the direct establishment of orientation relationships between the product phases and the initial muscovite is not possible because the muscovite totally disappeared during the first 5 min at 1175 °C. However, we can attempt to infer the original crystallographic orientations from the mutual arrangement of the product phases.

Basal sections of our heated muscovite grains, observed by SEM (Fig. 5), clearly show that the acicular crystals of γ-Al_2O_3 are oriented along three directions at 120° parallel to the former $(001)_{musc}$. Mullite rods are oriented along one preferential direction at 30° and 90° to these γ-Al_2O_3 directions. The XRD investigation of Eberhart (1963) and the detailed TEM study of Rodriguez-Navarro et al. (2003) demonstrated that the **c**-axes (direction of elongation) of the mullite crystals are oriented systematically parallel to the **b**-direction of the muscovite. Assuming that $\mathbf{c}_{mul}$ is parallel to the **b** direction of the former muscovite in our samples would imply that the γ-Al_2O_3 needles are elongated along the three equivalent **a**-directions of the former muscovite layer, with $[110]_{spinel}$ // $[100]_{musc}$. It is thus possible to deduce the orientation of the former muscovite from the orientation of the product phases, as illustrated by the scheme of Figure 9. This reconstruction also explains why mullite rods are seen as square or rectangular sections, when observed on lateral muscovite sections cut parallel to the γ-Al_2O_3 needles. It must be noted that, contrary to Rodriguez-Navarro et al. (2003) who reported mullite oriented along $[010]_{musc}$ or the symmetrically equivalent $<310>_{musc}$ directions, we observed only one preferential orientation for mullite in our samples (Fig. 5). The orientation of mullite with respect to γ-Al_2O_3, as seen in Figure 6b, is consistent with the orientation of mullite with respect to $(001)_{musc}$ described by Rodriguez-Navarro et al. (2003, see their Fig. 8). We cannot determine if $(111)_{spinel}$ was parallel to $(001)_{mica}$, but this orientation would be consistent with having three equivalent [110] directions of elongation of γ-Al_2O_3 at 120° parallel to $(001)_{musc}$. However, if we accept that the mullite rods are parallel to $\mathbf{b}_{musc}$, as discussed above, it follows that the [110] directions of elongation of γ-Al_2O_3 would be parallel to $\mathbf{a}_{musc}$, and this is not in accordance with the $[110]_{spinel}$ // $\mathbf{b}_{musc}$ topotactic relationships observed previously in heated muscovite by Eberhart (1963). If the γ-Al_2O_3 needles do have the topotactic orientation described by Eberhart (1963) and are elongated along [110], then it would imply that the mullite rods are oriented parallel to $\mathbf{a}_{musc}$ instead of $\mathbf{b}_{musc}$.

Morphology and growth of the product phases

The observed morphology of mullite is the usual one for this mineral. The dendritic habit we observed for short durations is also well documented by Rodriguez-Navarro et al. (2003), and indicative of rapid growth. It could result from two possible growth mechanisms: (1) a dendritic growth due to a local oversaturation controlled by diffusion (Kirkpatrick 1981; Baronnet 1984) or (2) the coalescence of mullite crystallites, as suggested by Rodriguez-Navarro et al. (2003). Whatever the growth mechanism, an evolution toward the usual equilibrium $\{110\} + \{\bar{1}10\}$ morphology is observed from 40 min by TEM, but hollow crystals are still observed by SEM up to 24 h. Similar skeletal mullite crystals were described by Brearley and Rubie (1990) from experiments at 750 °C, 1 kbar, for run durations of two weeks. These observations suggest that the formation of mullites with these characteristic dendritic to skeletal morphologies is a feature that appears to be typical of muscovite decomposition over quite a wide range of temperatures and pressures.

The acicular morphology of γ-Al_2O_3, on the other hand, is

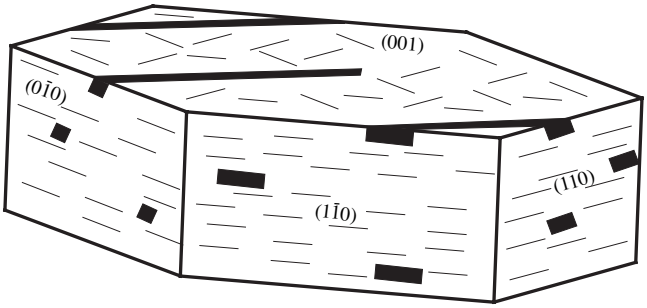

FIGURE 9. Schematic representation of the orientation relationships between γ-Al_2O_3 needles, blocky-looking mullite and the former muscovite, as reconstructed from petrographic microscopy, SEM, and TEM observations.

unexpected for a phase with an isometric spinel structure. Eberhart (1963) observed this spinel phase by TEM and reported a morphology of flattened octahedra. Our experiments differ from Eberhart's by being in strong disequilibrium conditions and with short heating durations, but this difference does not explain in itself the difference in morphology if the Al-rich oxide is indeed cubic. We are confident that our compound has been properly identified, being characterized by XRD, SAED patterns, and EDS microanalysis. Arguably, Gandolfi XRD patterns could be attributed to the related structures of other transition alumina compounds, some of which have non-isometric structures, but SAED patterns rather support the γ-Al_2O_3 identification. Moreover, γ-Al_2O_3 was reported by several authors as an early decomposition product of muscovite, whereas only Sundius and Byström (1953) report θ-Al_2O_3 as an intermediate phase in the transformation of γ- to α-Al_2O_3. It has been suggested that the γ-Al_2O_3 structure is not strictly cubic, but presents a tetragonal distortion (Gan and O'Connor 1996). Lee et al. (1999) and Lee et al. (2001) suggested a distorted symmetry for an Al-rich spinel phase from heated kaolinite. Tentatively, the anisotropy could be caused by an ordering of vacancies or Si in the γ-Al_2O_3 structure that would lower its symmetry. Such a preferential growth in some <110> directions, controlled by the symmetry of the alumina and not only by the muscovite precursor, may also explain the B needles lying at an angle to the basal planes of muscovite. Assuming γ-Al_2O_3 nuclei with $(111)_{spinel}$ // $(001)_{musc}$, there are six $<110>_{spinel}$ directions: three of them at 120° in the $(001)_{musc}$ basal plane, but also three making an angle of 45° with $(001)_{musc}$. Anisotropic growth along one of those $<110>_{spinel}$ directions that are not parallel to $(001)_{musc}$ may account for the B needles that were observed growing at an angle to the former muscovite cleavages.

Another possible explanation for the acicular morphology of γ-Al_2O_3 would be that it grew from an acicular precursor such as boehmite that would have formed during the very early stages of dehydration of the muscovite. Indeed, γ-Al_2O_3 is known to be the first transition alumina formed by the dehydration of boehmite (Wefers and Misra 1987; Zhou and Snyder 1991; Levin and Brandon 1998) and industrial γ-Al_2O_3 is actually synthesized this way. The transformation of boehmite to γ-Al_2O_3 is topotactic so the morphology of the nanoparticles remains unchanged (Krokidis et al. 2001; Digne et al. 2004; Toulhoat et al. 2005). The production of acicular γ-Al_2O_3 from boehmite has been described in a U.S. patent by Toulhoat et al. (1985).

For increasing durations, SEM observations (Figs. 3 and 4) indicate that the proportion of "clear" glass increases while the size of γ-Al_2O_3 crystals increases as their number decrease. Two hypotheses can be proposed to explain the growth of the needles: (1) their growth could result from coalescence as proposed by Rodriguez-Navarro et al. (2003) for mullite; or (2) Ostwald ripening (Ostwald 1900; Baronnet 1982; Cabane et al. 2001) could explain the resorption of the small needles to promote the growth of a few larger one. The presence of homogeneous glass around the larger needles and persistence of cloudy zones away from those at 24 h (Fig. 4c), and the disappearance of cloudy zones at 68 h, would be explained best by an Ostwald ripening mechanism.

CONCLUDING REMARKS

This study of muscovite destabilization for short durations revealed details about the reaction sequences that were not well documented from other experiments closer to equilibrium conditions. It also raises new questions about the much debated defect structure and nanotexture of the γ-Al_2O_3 phase. In addition to the importance for applied mineralogy, understanding the textures resulting from mica high-*T* transformations may provide further information about the transformations undergone by crustal xenoliths during their ascent, and thus constrain their thermal history.

ACKNOWLEDGMENTS

We are indebted to Adrian Brearley and Ralf Milke for their careful and constructive reviews of the manuscript. Assistance by M. Veschambre on the electron microprobe and by S. Nitsche on the transmission electron microscopy are gratefully acknowledged. We thank A. Baronnet for useful discussions. TEM work was performed at the CNRS-INSU French National Facility for electron microscopy at CRMCN, Marseille. K.D. expresses his thanks and gratitude to The Société de Secours des Amis des Sciences and to the Laboratoire Environnement et Minéralurgie, ENSG, CNRS-UMR 7569 for the grants.

REFERENCES CITED

Barlow, S.G. and Manning, D.A.C. (1999) Influence of time and temperature on reactions and transformations of muscovite mica. British Ceramic Transactions, 98, 122–126.

Baronnet, A. (1982) Ostwald ripening in solution; the case of calcite and mica. Estudios Geologicos, 38, 185–198.

——— (1984) Growth kinetics of the silicates. A review of basic concepts. Fortschritte der Mineralogie, 62, 187–232.

Brearley, A.J. (1986) An electron optical study of muscovite breakdown in pelitic xenoliths during pyrometamorphism. Mineralogical Magazine, 50, 385–397.

Brearley, A.J. and Rubie, D.C. (1990) Effects of H_2O on the disequilibrium breakdown of muscovite+quartz. Journal of Petrology, 31, 925–956.

Brindley, G.W. and Lemaître, J. (1987) Thermal, oxidation and reduction reactions of clay minerals. In A.C.D. Newman, Ed., Chemistry of clays and clay minerals, p. 319–370. Mineralogical Society Great Britain Monograph, 6, London.

Brindley, G.W. and Maroney, D. (1960) High-temperature reactions of clay mineral mixtures and their ceramic properties: II, reactions of kaolinite-mica-quartz mixtures compared with the K_2O-Al_2O_3-SiO_2 equilibrium diagram. Journal of the American Ceramic Society, 43, 511–516.

Brindley, G.W. and Nakahira, M. (1959) The kaolinite-mullite reaction series: I, Survey of outstanding problems. II, Metakaolin. III, The high-temperature phases. Journal of the American Ceramic Society, 42, 311–324.

Cabane, H., Laporte, D., and Provost, A. (2001) Experimental investigation of the kinetics of Ostwald ripening of quartz in silicic melts. Contributions to Mineralogy and Petrology, 142, 361–373.

Cameron, W.E. (1977) Mullite: a substituted alumina. American Mineralogist, 62, 747–755.

Cultrone, G., Rodriguez-Navarro, C., Sebastian, E., Cazalla, O., and de la Torre, M.J. (2001) Carbonate and silicate phase reactions during ceramic firing. European Journal of Mineralogy, 13, 621–634.

Deer, W.A., Howie, R.A., and Zussman, J. (1982) Rock-forming minerals (2nd edition). Vol 1A, Orthosilicates. Longmans, London.

Devineau, K. (2002) Déstabilisation haute température de poudres granitiques : Evolution des propriétés minéralogiques et physiques, 334 p. Ph.D. thesis, Institut National Polytechnique de Lorraine, Vandoeuvre-les-Nancy, France.

Devineau, K., Pichavant, M., and Villiéras, F. (2005) Melting kinetics of granitic powder aggregates at 1175°C, 1 atm. European Journal of Mineralogy, 17, 387–398.

Digne, M., Sautet, P., Raybaud, P., Euzen, P., and Toulhoat, H. (2004) Use of DFT to achieve a rational understanding of acid-basic properties of γ-alumina surfaces. Journal of Catalysis, 226, 54–68.

Eberhart, J. (1963) Transformation de la muscovite par chauffage entre 700 et 1200°C. Bulletin Société Française Minéralogie Cristallographie, 86, 213–251.

Gan, B.K. and O'Connor, B.H. (1996) Structure refinement of gamma alumina-Revisited. XVII Congress and General Assembly of the International Union of Cristallography, Abstract, Aug 8–17, Seattle, Washington.

Grapes, R.H. (1986) Melting and Thermal Reconstitution of Pelitic Xenoliths, Wehr Volcano, East Eifel, West Germany. Journal of Petrology, 27, 343–396.

Gutiérrez, G., Taga, A., and Johansson, B. (2001) Theoretical structure determination of γ-Al_2O_3. Physical Review B, 65, 0121011–0121014.

Han, L., Jun-Qiao, W., and Ji-Zhou, C. (1995) Structure imperfection of γ-Al_2O_3. Polyhedron, 14, 445–449.

Kingery, W.D., Bowen, H.K., and Uhlmann, D.R. (1976) Introduction to Ceramics, 1032 p. Wiley, New York.

Kirkpatrick, R.J. (1981) Kinetics of crystallisation of igneous rocks. In R.J. Kirkpatrick and A.C. Lasaga, Eds., Kinetics of geochemical processes, vol. 8, p. 321–395. Reviews in Mineralogy, Mineralogical Society of America, Chantilly, Virginia.

Krokidis, X., Raybaud, P., Gobichon, A.E., Rebours, B., Euzen, P., and Toulhoat, H. (2001) Theoretical study of the dehydration process of Boehmite to γ-alumina. Journal of Physical Chemistry B, 105, 5121–5130.

Kryukova, G.N., Klenov, D.O., Ivanova, A.S., and Tsybulya, S.V. (2000) Vacancy ordering in the structure of γ-Al_2O_3. Journal of the European Ceramic Society, 20, 1187–1189.

Lee, S., Kim, Y.J., and Moon, H.S. (1999) Phase transformation sequence from kaolinite to mullite investigated by an energy-filtering transmission electron microscope. Journal of the American Ceramic Society, 82, 2841–2848.

Lee, S., Kim, Y.J., Lee, H.J., and Moon, H.S. (2001) Electron-beam-induced phase transformations from metakaolinite to mullite investigated by EF-TEM and HRTEM. Journal of the American Ceramic Society, 84, 2096–2098.

Leonard, A.J. (1977) Structural analysis of the transition phases in the kaolinite-mullite thermal sequence. Journal of the American Ceramic Society, 60, 37–43.

Levin, I. and Brandon, D. (1998) Metastable alumina polymorphs: crystal structures and transition sequences. Journal of the American Ceramic Society, 81, 1995–2012.

Low, I.M. and McPherson, R.R. (1988) The structure and composition of Al-Si spinel. Journal of Materials Science Letters, 7, 1196–1198.

Mackenzie, K.J.D., Brown, I.W.N., Cardile, C.M., and Meinhold, R.H. (1987) The thermal reactions of muscovite studied by high resolution solid-state 29-Si and 27-Al NMR. Journal of Materials Science, 22, 2645–2654.

McHale, J.M., Yürekli, K., Dabbs, D.M., Navrotsky, A., Sundaresan, S., and Aksay, A.I. (1997) Metastability of spinel-type solid solutions in the SiO_2-Al_2O_3 system. Chemistry of Materials, 9, 3096–3100.

Nicol, A.W. (1964) Topotactic transformation of muscovite under mild hydrothermal conditions. Clays and Clay Minerals, 12, 11–19.

Ostwald, W. (1900) Uber die vemeintliche isomerie des roten und gelben queck-silberoxyds und die oberflachen-spannung fester korper. Zeitschrift für Physikalische Chemie, 34, 495–512.

Paquette, J.L., Goncalves, P., Devouard, B., and Nicollet, C. (2004) Micro-drilling ID-TIMS U-Pb dating of single monazites: A new method to unravel complex poly-metamorphic evolutions. Application to the UHT granulites of Andriamena (North-Central Madagascar). Contributions to Mineralogy and Petrology, 147, 110–122.

Pichavant, M. and Manning, D.A.C. (1984) Petrogenesis of tourmaline granites and topaz granites: the contribution of experimental data. Physics of the Earth and Planetary Interiors, 35, 31–50.

Putnis, A. and McConnell, J.D.C. (1980) Principles of Mineral Behaviour, 257 p. Blackwell Scientific Publications, Oxford.

Rodriguez-Navarro, C., Cultrone, G., Sanchez-Navas, A., and Sebastian, E. (2003) TEM study of mullite growth after muscovite breakdown. American Mineralogist, 88, 713–724.

Roy, R. (1949) Decomposition and resynthesis of the micas. Journal of the American Ceramic Society, 32, 202–209.

Rubie, D.C. and Brearley, A.J. (1987) Metastable melting during the breakdown of muscovite + quartz at 1 kbar. Bulletin de Minéralogie, 110, 533–549.

Sanchez-Navas, A. (1999) Sequential kinetics of a muscovite-out reaction: A natural example. American Mineralogist, 84, 1270–1286.

Souza-Santos, P., Souza-Santos, H., and Toledo, S.P. (2000) Standard transition aluminas. Electron microscopy studies. Materials Research, 3, 104–114.

Srikrishna, K., Thomas, G., Martinez, R., Corral, M.P., de Aza, S., and Moya, J.S. (1990) Kaolinite-mullite reaction series: a TEM study. Journal of Materials Science, 25, 607–612.

Sundius, N. and Byström, A.M. (1953) Decomposition products of muscovite at temperatures between 1000 and 1260°C. Transactions of the British Ceramic Society, 52, 632–642.

Tite, M.S. and Maniatis, Y. (1975) Examination of ancient pottery using the scanning electron microscope. Nature, 257, 122–123.

Toulhoat, H., Jacquin, Y., and Dupin, T. (1985) Supported catalyst of increased resistance to poisons, useful for hydrotreating metal-containing oil fractions. U.S. Patent No. 4,499,203.

Toulhoat, H., Digne, M., Arrouvel, C., and Raybaud, P. (2005) DFT studies of fluid-minerals interactions at the molecular level: examples and perspectives. Oil & Gas Science and Technology, 60, 417–433.

Wefers, K. and Misra, C. (1987) Oxides and hydroxides of Aluminum. Alcoa Laboratories, Pittsburgh, Pennsylvania.

Worden, R.H., Champness, P.E., and Droop, G.T.R. (1987) Transmission electron microscopy of the pyrometamorphic breakdown of phengite and chlorite. Mineralogical Magazine, 51, 107–121.

Yoder, H.S. and Eugster, H.P. (1955) Synthetic and natural muscovites. Geochimica et Cosmochimica Acta, 8, 225–280.

Zhou, R.S. and Snyder, R.L. (1991) Structures and transformation mechanisms of the eta, gamma and theta transitions aluminas. Acta Crystallographica, B 47, 617–630.

MANUSCRIPT RECEIVED MARCH 3, 2005
MANUSCRIPT ACCEPTED AUGUST 26, 2005
MANUSCRIPT HANDLED BY JOHN AYERS